

University of Wollongong

Research Online

---

Australian Institute for Innovative Materials -  
Papers

Australian Institute for Innovative Materials

---

1-1-2015

## A versatile binder-free TiO<sub>2</sub> paste for dye-sensitized solar cells

Jeremy H. Yune  
ANSTO

Inna Karatchevtseva  
ANSTO

P Evans  
Australian Nuclear Science And Technology Organisation

Klaudia K. Wagner  
University of Wollongong, kwagner@uow.edu.au

Matthew J. Griffith  
University of Wollongong, mjg48@uow.edu.au

*See next page for additional authors*

Follow this and additional works at: <https://ro.uow.edu.au/aiimpapers>

 Part of the [Engineering Commons](#), and the [Physical Sciences and Mathematics Commons](#)

---

### Recommended Citation

Yune, Jeremy H.; Karatchevtseva, Inna; Evans, P; Wagner, Klaudia K.; Griffith, Matthew J.; Officer, David L.; and Triani, Gerry, "A versatile binder-free TiO<sub>2</sub> paste for dye-sensitized solar cells" (2015). *Australian Institute for Innovative Materials - Papers*. 1420.  
<https://ro.uow.edu.au/aiimpapers/1420>

Research Online is the open access institutional repository for the University of Wollongong. For further information contact the UOW Library: [research-pubs@uow.edu.au](mailto:research-pubs@uow.edu.au)

---

## A versatile binder-free TiO<sub>2</sub> paste for dye-sensitized solar cells

### Abstract

In this study, binder-free TiO<sub>2</sub> colloidal pastes have been prepared using a variety of heterocyclic bases with diverse characteristics to produce robust photoanodes for dye-sensitized solar cells (DSSC) from a single cast film thickness of 5 micron. The influence of the base on the electrode structure and film morphology, including its electron donor characteristics are investigated after low temperature thermal treatment and high temperature sintering. The results show that quinoline in the TiO<sub>2</sub> paste is retained within the electrode structure in comparison to piperidine and pyridine after a short thermal treatment of 150 °C for 15 minutes. The presence of organic additives with  $\pi$ -conjugation in the photoanode enhances both electron injection efficiency and charge carrier lifetime resulting in higher  $J_{SC}$  and  $V_{OC}$ . This formulation in combination with low temperature processing yields an energy conversion efficiency of over 5% in DSSC devices. In devices where high temperature sintering is permitted, the performance of TiO<sub>2</sub> electrodes converges towards an efficiency of over 6%, irrespective of the organic additive within the paste. This formulation offers a high degree of versatility in casting electrodes onto polymer, glass or metal foil substrates from a single source of TiO<sub>2</sub> paste, for the many variants of low-cost solar cells.

### Keywords

sensitized, dye, paste, tio2, free, binder, versatile, solar, cells

### Disciplines

Engineering | Physical Sciences and Mathematics

### Publication Details

Yune, J. H., Karatchevtseva, I., Evans, P. J., Wagner, K., Griffith, M. J., Officer, D. & Triani, G. (2015). A versatile binder-free TiO<sub>2</sub> paste for dye-sensitized solar cells. *RSC Advances: an international journal to further the chemical sciences*, 5 (37), 29513-29523.

### Authors

Jeremy H. Yune, Inna Karatchevtseva, P Evans, Klaudia K. Wagner, Matthew J. Griffith, David L. Officer, and Gerry Triani



CrossMark  
 click for updates

Cite this: *RSC Adv.*, 2015, 5, 29513

## A versatile binder-free TiO<sub>2</sub> paste for dye-sensitized solar cells†

Jeremy H. Yune,<sup>a</sup> Inna Karatchevtseva,<sup>a</sup> Peter J. Evans,<sup>a</sup> Klaudia Wagner,<sup>b</sup> Matthew J. Griffith,<sup>b</sup> David Officer<sup>b</sup> and Gerry Triani<sup>\*a</sup>

In this study, binder-free TiO<sub>2</sub> colloidal pastes have been prepared using a variety of heterocyclic bases with diverse characteristics to produce robust photoanodes for dye-sensitized solar cells (DSSC) from a single cast film thickness of 5 micron. The influence of the base on the electrode structure and film morphology, including its electron donor characteristics are investigated after low temperature thermal treatment and high temperature sintering. The results show that quinoline in the TiO<sub>2</sub> paste is retained within the electrode structure in comparison to piperidine and pyridine after a short thermal treatment of 150 °C for 15 minutes. The presence of organic additives with  $\pi$ -conjugation in the photoanode enhances both electron injection efficiency and charge carrier lifetime resulting in higher  $J_{sc}$  and  $V_{oc}$ . This formulation in combination with low temperature processing yields an energy conversion efficiency of over 5% in DSSC devices. In devices where high temperature sintering is permitted, the performance of TiO<sub>2</sub> electrodes converges towards an efficiency of over 6%, irrespective of the organic additive within the paste. This formulation offers a high degree of versatility in casting electrodes onto polymer, glass or metal foil substrates from a single source of TiO<sub>2</sub> paste, for the many variants of low-cost solar cells.

Received 10th November 2014

Accepted 19th March 2015

DOI: 10.1039/c4ra14247k

[www.rsc.org/advances](http://www.rsc.org/advances)

### Introduction

One of the major global challenges over the next 40 years will be to fulfill the rising energy demands from emerging countries and an increasing population.<sup>1</sup> Solar generation has the potential to contribute a large proportion of the renewable energy required for the projected 30 terawatts by 2050.<sup>2,3</sup> However, in order for solar to achieve better penetration into the energy sector, a more competitive cost structure is required to lower the cost of manufacture.<sup>4</sup> Dye-sensitized solar cells are a promising low-cost third generation photovoltaic device where both components and manufacturing processes are relatively cheaper in comparison to silicon based devices<sup>5</sup> and have demonstrated an energy conversion efficiency of over 10% (ref. 6) coupled with good performance over a broad range of light intensity levels.<sup>7,8</sup>

Since the pioneering work of O'Regan and Gratzel in 1991,<sup>9</sup> dye-sensitized solar cells (DSSC) have created enormous interest in the research community, where improvements in both

materials and process technologies have been addressed along with enhancements in device architecture.

These developments have translated into an exponential rise in peer-review articles<sup>10</sup> resulting in performance improvements, which have yielded devices with energy conversion efficiencies of 15%.<sup>11</sup> One of the prime areas of research has been the development of TiO<sub>2</sub> electrodes in DSSC, which are typically deposited as a continuous film from a viscous paste. TiO<sub>2</sub> paste is prepared with organic binders, which modify the rheology for coating and impart porosity in the thick film structure.

Conducting glass substrates are used as the support and these allow thermal process treatments at temperatures >400 °C to ensure organics are eliminated and to improve particle binding and adhesion to the substrate.<sup>6</sup> A key driver in cost reduction of the DSSC is the replacement of glass-based substrates with polymers that are amenable to continuous roll-to-roll processing.<sup>12,13</sup> Low temperature mesoporous TiO<sub>2</sub> films for photoanodes on polymers require processes less than 150 °C with acceptable particle connectivity for electron diffusion. Several methods have been reported as low temperature processes with additional steps following TiO<sub>2</sub> film formation. They include immersion with TiCl<sub>4</sub>,<sup>14</sup> UV-O<sub>3</sub> curing,<sup>15-17</sup> TiO<sub>2</sub> atomic layer deposition<sup>18</sup> or compression.<sup>19</sup> All of these studies show improvements in performance after TiO<sub>2</sub> film deposition, with the best recorded efficiency of 7.6% (ref. 20) on ITO/PEN achieved by compression coupled with UV-O<sub>3</sub> curing post film formation. However, integration of such a process in DSSC device fabrication remains challenging<sup>12</sup> where a singular

<sup>a</sup>Institute of Materials Engineering, Australian Nuclear Science and Technology Organisation (ANSTO), Locked Bag 2001, Kirrawee DC, NSW 2232, Australia. E-mail: gtx@ansto.gov.au; Tel: +61 2 97179070

<sup>b</sup>ARC Centre of Excellence for Electromaterials Science and Intelligent Polymer Research Institute, AIMM Facility, University of Wollongong, Wollongong, NSW 2522, Australia

† Electronic supplementary information (ESI) available. See DOI: 10.1039/c4ra14247k

process step following deposition with minimal resident time is preferred.<sup>13</sup>

Casting of TiO<sub>2</sub> from a viscous vehicle onto substrates is by far the preferred method of depositing electrodes for DSSC.<sup>12,21</sup> However, additives for low temperature TiO<sub>2</sub> paste must provide adequate viscosity and volatility in order to yield uniform porous structures. An interesting method reported by Park *et al.*<sup>22,23</sup> utilises a binder-free formulation by adding small quantities of ammonia solution into an acidic TiO<sub>2</sub> aqueous sol. Surface mediated CH<sub>3</sub>COO<sup>-</sup>/NH<sub>4</sub><sup>+</sup> couples are formed within the slurry, which results in the reduction of the double layer repulsion between the particles; as a result this induces TiO<sub>2</sub> particles to flocculate sufficiently to allow uniform films to be cast.

In our previous study,<sup>24</sup> the influence of acetate molar ratio within the acidic TiO<sub>2</sub> colloid was investigated in low temperature processing of electrodes in DSSC. Lowering the molar ratio of TiO<sub>2</sub> to CH<sub>3</sub>COOH in the starting colloid and the amount of ammonia in the paste formation, followed by low temperature processing at 150 °C for 15 minutes, resulted in the energy conversion efficiency of the DSSC increasing from 2.83 to 5.00% in comparison to Park's results.<sup>22,23</sup> Further incremental improvements were possible after the electrodes were heat treated at 150 °C for 24 hours.

Huang<sup>25</sup> and Boschloo<sup>26</sup> have both reported enhancements in device performance by the addition of particular nitrogen-containing compounds to the electrolyte solution. For example, the use of 4-*tert*-butylpyridine (TBP) as documented in the literature enhances the performance of the cell by improving the open-circuit voltage but at the expense of  $J_{sc}$ .<sup>25</sup> The proposed mechanism is that TBP binds to either a TiO<sub>2</sub> surface or electrolyte *via* the nitrogen atom thus protecting it against the charge recombination. The basic nature and electron donor properties of various heterocyclic amines within the electrolyte have been identified to be responsible of TiO<sub>2</sub> conduction band shift and therefore influence DSSC characteristics.<sup>27–31</sup>

In this study, we investigate the incorporation of a variety of bases with diverse characteristics, including basicity, boiling point and electrochemical properties. TiO<sub>2</sub> colloidal pastes were formulated using heterocyclic amines during paste preparation as opposed to addition within the electrolyte, with anticipation that this functional moiety will have a higher probability of binding to a TiO<sub>2</sub> surface, hence reducing back electron transfer. This study seeks to establish a relationship between electron donor characteristics of the base in the TiO<sub>2</sub> electrode and the solar cell performance of DSSCs prepared with several amines; piperidine, pyridine and quinoline. In order to best compare the high temperature and low temperature paste performance in DSSCs, we have fabricated DSSCs with a single nanocrystalline TiO<sub>2</sub> layer on a glass photoanode without the usual blocking layer (Fig. 1).

## Experimental

### Preparation of TiO<sub>2</sub> paste

TiO<sub>2</sub> solutions were prepared using a method reported by Karatchevtseva *et al.*<sup>32</sup> Briefly, 85 mL of titanium(IV) isopropoxide

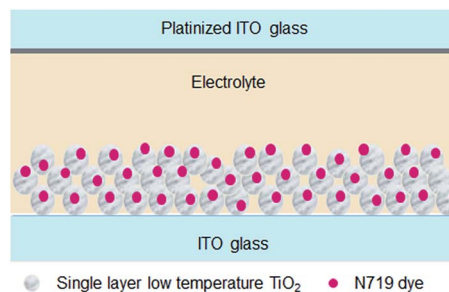


Fig. 1 Schematic diagram of the DSSC structure used in these studies.

was mixed with 17.4 g of glacial acetic acid (1 : 1 mol ratio) in a glove box under inert conditions and vigorous stirring. This solution was slowly added *via* a dropping funnel to 512 g of H<sub>2</sub>O under vigorous stirring for 10 minutes at room temperature followed by the addition of 5 mL of nitric acid (concentration 69%), used as a peptization agent.<sup>33,34</sup> The reaction mixture was heated at 80 °C under vigorous stirring for 8 hours. TiO<sub>2</sub> sol was converted into highly crystalline anatase *via* a hydrothermal procedure by introducing 150 g of TiO<sub>2</sub> sol into a 200 mL titanium autoclave heated to 240 °C, which was controlled by ramping at 2 °C min<sup>-1</sup> and held at temperature for 14 hours. An aqueous TiO<sub>2</sub> suspension of anatase with uniform particle size distribution was collected after ultra-sonication for 15 minutes followed by centrifugal separation at a rotation speed of 3000 min<sup>-1</sup> for 15 minutes.

Binder-free TiO<sub>2</sub> paste was prepared by adding a calculated quantity of dilute 2 M basic solution to an acidic anatase TiO<sub>2</sub> colloid where the final weight percentage of TiO<sub>2</sub> was 21%. This was determined after thermogravimetric analysis where the amount of base (piperidine, pyridine and quinoline) was in the range 1.7–2.1 wt% with respect to TiO<sub>2</sub>. Viscous pastes were ready for casting after 2 hours of agitation.

### DSSC preparation

The TiO<sub>2</sub> photoanode films were deposited by casting onto either microscope soda lime glass slides or indium doped tin oxide (ITO) coated on glass substrates (Asahi, sheet resistance:  $R_s \leq 8 \Omega \text{ sq}^{-1}$ ) using the doctor blade technique. The thickness of a single cast dried TiO<sub>2</sub> electrode was  $5.0 \pm 0.2 \mu\text{m}$ . The TiO<sub>2</sub> films were first air dried for 30 minutes and then heat-treated on a hot plate at either 150 °C for 15 minutes for low temperature devices or processed at 450 °C for 30 minutes. The active electrode area was 0.25 cm<sup>2</sup>. Prior to assembly into DSSC devices, the TiO<sub>2</sub> films were further treated for 2 hours at 120 °C on a hot plate, in order to remove most of physisorbed water, and immersed while hot into 0.3 mM anhydrous *cis*-diisothiocyanato-bis(2,2'-bipyridyl-4,4'-dicarboxylato)ruthenium(II)bis(tetrabutylammonium) (N719 dye purchased from Solaronix SA Ltd.) solution in acetonitrile/*tert*-butyl alcohol (1/1) for 22 hours. The sensitized TiO<sub>2</sub> electrode was sandwiched with a Pt-sputtered (~30 nm thickness) indium tin oxide (ITO)-glass counter electrode (Delta Technologies,  $R_s \sim 10 \Omega \text{ sq}^{-1}$ ) spaced with a 25  $\mu\text{m}$  Surlyn sealant (Fig. 1). An electrolyte solution comprising 0.6 M 1,2-dimethyl-3-propylimidazolium iodide

(DMPII), 0.5 M 4-*tert*-butylpyridine, 0.1 M LiI, and 0.05 M I<sub>2</sub> in a solvent mixture of 85 : 15 acetonitrile/valeronitrile was injected between the electrodes through a hole in the counter electrode by a vacuum-filling procedure. Four samples were prepared for every condition investigated.

### TiO<sub>2</sub> film characterisation

The thickness of both dried and thermally treated TiO<sub>2</sub> films on glass were measured using the Alpha-Step IQ Surface Profiler (KLA-Tencor). Further, measurements of film transmittance were recorded by UV-Vis spectroscopy on a Perkin Elmer Lambda 35 UV-Vis spectrometer.

Specific surface areas of the as-prepared and post-treated TiO<sub>2</sub> electrodes were measured by the Brunauer–Emmett–Teller (BET) nitrogen adsorption method. Cast films were removed from their substrates by scratching and placing contents into glass bulbs for measurement. Nitrogen adsorption isotherms at 77 K were measured on a Quantachrome AutoSorb iQ volumetric adsorption analyzer.

Scanning electron microscopy (SEM) provided a comparative study of TiO<sub>2</sub> film morphology. Samples were examined by field emission SEM (Zeiss Supra 55VP) operating at an accelerating voltage of 10 kV. Films were mounted on a conductive carbon adhesive and approximately 30 Å of platinum was evaporated onto the surface to prevent charging.

Fourier transform infrared (FTIR) spectra were obtained on a Nicolet Nexus 8700 FTIR spectrometer (Thermo Electron Corporation, Madison, WI). Both dried and thermally treated films were measured using the Smart iTR™ sampling accessory to observe the presence of residual organics. Spectra were collected by averaging 32 scans with a nominal resolution of 4 cm<sup>-1</sup>.

### DSSC characterisation

Current–voltage curves were recorded using a Keithley 2400 source measure unit after illuminating the DSSCs with a simulated 100 mW cm<sup>-2</sup> air mass AM 1.5 light source (Oriel) equipped with a KG5 filter to remove longer wavelengths. The light intensity was adjusted using a calibrated silicon diode (Peccell). The device area was masked with black paint defining an aperture slightly larger than the active area.<sup>35</sup> The light intensity of the simulated sunlight source was reduced for specific measurements using neutral density filters. Incident photon-to-current conversion efficiency (IPCE) spectra were recorded on a home-built set-up using the monochromated output from a xenon lamp equipped with sorting filters. The output beam was focused to a spot size smaller than the DSSC area. The short circuit current response of devices was recorded in 5 nm steps using the aforementioned Keithley 2400 instrument referenced to the output of a calibrated silicon diode (Peccell).

Electron lifetime and diffusion coefficient measurements were performed using stepped light-induced recording of photocurrent and photo-voltage (SLIM-PCV) transients.<sup>36</sup> Measurements were performed using a 635 nm diode laser illuminating the entire DSSC active area. This wavelength was selected as the dyes are weakly absorbing at 635 nm, allowing a uniform generation of electron density throughout the entire

TiO<sub>2</sub> film thickness. The illumination intensity of the laser, controlled by the input voltage, produced values ranging from 2 mW cm<sup>-2</sup> to 35 mW cm<sup>-2</sup>. Photocurrent and photovoltage transients were induced by the small stepwise (≤10%) change of the laser intensity, controlled with a PC using a digital-to-analogue converter. Induced transients were measured by a fast multimeter (AD7461A, Advantest). Electron densities at specific laser illumination intensities were determined by a charge extraction method in which the light source was switched off at the same time the DSSC device was switched from open to short circuit.<sup>35</sup> The resulting current was integrated, with the electron density calculated from the amount of charge extracted. Diffusion coefficients were determined by fitting the current decays to a single exponential as previously reported,<sup>36</sup> although we note that this treatment neglects potential recombination losses during charge transport. Electron lifetimes were determined by fitting the voltage transients to single exponential decays as previously reported.<sup>36</sup>

The electrochemical data were obtained using square wave voltammetry in anhydrous acetonitrile containing 0.1 M tetrabutylammonium perchlorate (TBAP) as supporting electrolyte. The working electrodes were indium tin oxide (ITO) slides with N719-sensitised TiO<sub>2</sub>. Solutions were degassed prior to measurement and ferrocene was added as an internal reference. Pt mesh and Ag/Ag<sup>+</sup> electrode were used as the counter electrode and quasi-reference electrode respectively. Half-wave potential was measured for 1 mM ferrocene,  $E_{1/2} = 0.21$  V, vs. Ag/Ag<sup>+</sup> reference electrode. The results were recorded using an eDAQ potentiostat system controlled by eDAQ EChem software. Solutions were degassed prior the measurements.

HOMO potentials were estimated from the oxidation half-wave potential ( $E_{1/2}^{ox}$ ) of the anodic peak. The optical band gap was estimated from UV-Vis absorption spectra of the samples prior to electrochemistry. The LUMO potentials for both dyes were then estimated by subtracting the optical band gap value from the HOMO potential.

Fluorescence spectra were recorded with a Horiba Scientific Fluorolog Model FL 3-221 spectrofluorometer system.

## Results and discussion

TiO<sub>2</sub> pastes were formulated with the addition of a heterocyclic base to the starting acidic TiO<sub>2</sub> colloid and processed according to our previous study.<sup>24</sup> Briefly, the base reacts with residual acetic acid groups and forms a salt. An increase in ion concentration between the acid<sup>-</sup>/base<sup>+</sup> couple promotes a decrease of the double layer repulsion between TiO<sub>2</sub> nanoparticles thereby contributing to flocculation, which results in the formation of a viscous slurry. A similar behaviour was reported in our previous study where an optimum weight ratio between the additive base and TiO<sub>2</sub> content was defined. A similar approach was undertaken in this study.

### TiO<sub>2</sub> films properties

The presence of organics was monitored by Fourier-Transform Infrared (FTIR) spectroscopy. FTIR spectra of piperidine,



pyridine and quinoline-based TiO<sub>2</sub> as-prepared films are shown in Fig. 2. Several common IR adsorption bands were observed in each sample. Firstly, the broad band below 800 cm<sup>-1</sup> is due to the formation of an extensive inorganic Ti–O–Ti network. A broad peak centred at ~1630 cm<sup>-1</sup> indicates the presence of Brønsted acidity (the O–H groups residing on TiO<sub>2</sub> surface) in all samples. While another broad doublet peak centred between 1500 and 1300 cm<sup>-1</sup> is indicative of the Lewis acidity.

The nature of acid sites may be defined by the presence of surface protons leading to the Brønsted sites or cationic centres due to unsaturation in coordination, which explains the Lewis acidity. These sites can potentially serve as the adsorption sites for organic species. For example, Miyata *et al.*<sup>37</sup> observed a broad band in the region 1300–1400 cm<sup>-1</sup> in their study of pyridine adsorbed on transition metal oxides. Dines *et al.*<sup>38</sup> have reported bands at similar wavenumbers in the case of quinoline chemisorbed onto TiO<sub>2</sub> surface.

There are also several IR bands found in each spectrum that are unique to each sample. For example, quinoline typically has 3 characteristic bands (due to aromatic ring vibration) near 1600 cm<sup>-1</sup>, two of which, 1600 and 1565 cm<sup>-1</sup>, can clearly be seen in the spectrum (Fig. 2a). In pyridine (Fig. 2b), the interactions between ring C=C and C=N stretching vibrations result in two absorption bands found at 1546 and 1489 cm<sup>-1</sup>, respectively.<sup>39</sup> Piperidine has a distinct absorption band at 1028 cm<sup>-1</sup> that has been assigned to the C–N stretching vibration (Fig. 2c).

After casting the TiO<sub>2</sub> paste into thick films, electrodes were heat treated at 150 °C to prepare the anode for subsequent solar cell fabrication. FTIR spectra of TiO<sub>2</sub> films treated at 150 °C for 15 minutes are shown in Fig. 3. The IR data indicated that only the quinoline-based film retained most of its organic component after this heat treatment, with characteristic bands distinguishable in the spectrum (Fig. 3a).

In contrast, the intensity of IR bands for both pyridine and piperidine treated at 150 °C for 15 minutes (Fig. 3b and c) have

significantly decreased compared to the corresponding as-prepared films. This is due to desorption of pyridine or piperidine since their boiling points are around 115 and 106 °C, respectively. In comparison, the spectrum of the quinoline based paste shows little change following treatment at 150 °C as the boiling point of quinoline is 238 °C.

After continuous heat treatment at 450 °C for 30 min all three samples produced almost identical IR spectra (Fig. 4). Firstly, a minor peak is evident in all samples in the range 1020–1015 cm<sup>-1</sup> and attributed to a residual carbon. The CHN microanalytical analysis indicated the atomic percentage of carbon for quinoline, pyridine and piperidine-based films heat treated at 450 °C for 30 min were 0.15, 0.19 and 0.18, respectively. Secondly, the presence of a weak broad peak at 1640 cm<sup>-1</sup>, corresponding to O–H deformation, indicates that surface bonded hydroxyl groups were still present even after the heat treatment at 450 °C. This suggests the chemical functionality of the TiO<sub>2</sub> surface appears largely unchanged after the prescribed thermal treatments.

It is well established that the TiO<sub>2</sub> photoanode microstructure affects the maximum amount of dye loading on the TiO<sub>2</sub> electrodes, in addition to influencing device physics such as electron diffusion and charge carrier lifetime. Moreover, several reports suggested that the mesoscopic structure of the TiO<sub>2</sub> electrodes had a major influence on the performance of DSSCs.<sup>40–42</sup> Surface area and porosity as well as particle size distribution and film preparation procedure<sup>43,44</sup> could all have a major influence on film morphology and therefore affect the structure of TiO<sub>2</sub> electrode. Thus in this work the morphologies of TiO<sub>2</sub> films prepared using different bases and post-treatment conditions were carefully studied.

Fig. 5 shows plan view SEM images of titania films prepared using different pastes. The morphology of the resulting TiO<sub>2</sub> films produced after heat treatment at 150 °C for 15 minutes appears to be similar, showing uniform porosity and interconnected nanoparticles throughout the film.

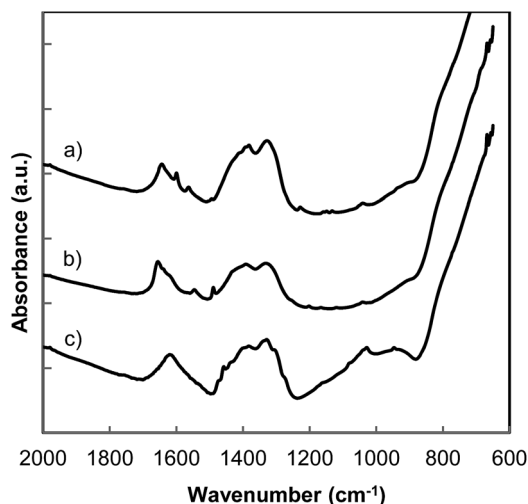


Fig. 2 FTIR spectra of as-prepared TiO<sub>2</sub> films synthesised using: (a) quinoline, (b) pyridine and (c) piperidine.

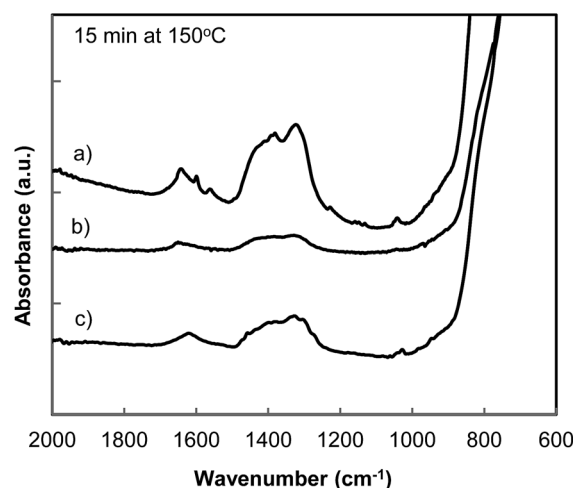


Fig. 3 FTIR spectra of TiO<sub>2</sub> films synthesised using: (a) quinoline, (b) pyridine and (c) piperidine after heat treated at 150 °C for 15 min.

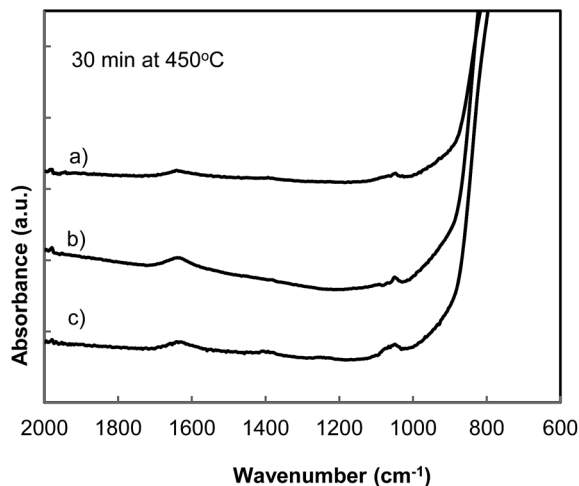


Fig. 4 FTIR spectra of TiO<sub>2</sub> films synthesised using: (a) quinoline, (b) pyridine and (c) piperidine after heat treated at 450 °C for 30 min.

Nitrogen sorption analysis was used to assess the effect of different heterocyclic bases have on TiO<sub>2</sub> film formation and porosity of the cast electrodes. A summary of this analysis detailing surface area and porosity of cast electrodes is presented in Table 1. Nitrogen adsorption–desorption isotherms for TiO<sub>2</sub> films post treated at 150 °C for 15 minutes and 450 °C at 30 minutes (not shown) have designated type IV isotherms using the IUPAC classification scheme.<sup>45</sup>

The isotherms in each heat-treatment group were of similar shape and all exhibited a narrow type H1 hysteresis loop over the relative pressure range 0.80–1.0, associated with the capillary condensation in mesopores. Surface area values estimated by the BET method for all films treated at 150 °C for 15 min were in the range 80.4–87.5 m<sup>2</sup> g<sup>-1</sup> and total pore volume 0.252–0.254 cm<sup>3</sup> g<sup>-1</sup>. A decrease in both surface area and pore volume was observed after sintering at 450 °C which was attributed to nanoparticle necking. These characteristics are comparable to low and high temperature TiO<sub>2</sub> electrodes developed by Miyasaka *et al.*<sup>46</sup> and Ito *et al.*,<sup>6</sup> respectively.

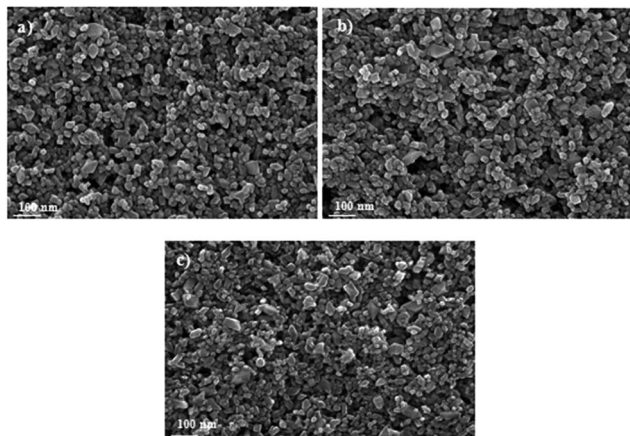


Fig. 5 SEM images of (a) piperidine, (b) pyridine and (c) quinoline-based TiO<sub>2</sub> films after 15 minutes at 150 °C.

Overall, very little difference in film morphology could be observed between the bases studied, suggesting that the nature of the bases used during the paste formulation does not influence significantly the microstructure of the TiO<sub>2</sub> electrodes.

### DSSC performance

TiO<sub>2</sub> electrodes were cast using additives piperidine, pyridine or quinoline formulated in pastes, followed by heat treatment to 150 °C. TiO<sub>2</sub> blocking layers were not used in the preparation of these devices. Since the porosities of the high and low temperature pastes are similar (Table 1), the back transfer recombination reaction between electrons in the ITO electrode and electrolyte ions penetrating through the TiO<sub>2</sub> pores should also be similar for both types of paste, allowing for an accurate comparison of the pastes. Cells were prepared after sensitization with ruthenium dye N719. Table 2 records DSSC performance after both low (150 °C) and high temperature (450 °C) treatment of films prepared with different heterocyclic bases: piperidine, a six membered ring amine; pyridine, a six membered ring amine with  $\pi$ -conjugated electron and quinoline films, which is more electron rich compared to pyridine *via* the supplementary aromatic. The order of basicity is as follows: piperidine > pyridine > quinoline.<sup>47</sup> Previously FTIR spectra suggested different amounts of base were retained within TiO<sub>2</sub> electrodes after heat treatment at 150 °C for 15 minutes since the boiling point of piperidine and pyridine is lower than this temperature. In order to study the influence of the base, which is responsible for the characteristic response in DSSC performance, films were prepared and performance tested without heat treatment where an equivalent amount of additive with a weight ratio of base to TiO<sub>2</sub> was between 1.7 and 2.1 wt%.

Table 2 summarises the DSSC performance data as a function of heat treatment. All films under investigation were approximately 5  $\mu$ m thick. The  $V_{oc}$  values for the as-prepared piperidine, pyridine and quinoline films were recorded at 753, 760 and 772 mV, respectively. This trend is in good agreement with previous results from Kusama *et al.*<sup>27</sup> where similar bases were adsorbed onto the TiO<sub>2</sub> surface from the electrolyte solution. In this study the changes were ascribed to modification of the TiO<sub>2</sub> conduction band, in accordance with other literature. Such shifts of the conduction band typically result in reduced device photocurrent as the driving force for charge injection between the dye LUMO and the TiO<sub>2</sub> conduction band is reduced.<sup>25</sup> However, in our study we observed that  $J_{sc}$  increases corresponding to increases in the  $\pi$ -electron strength of the bases. The  $J_{sc}$  improved significantly from 4.84, 7.51 to 8.12 mA cm<sup>-2</sup> for piperidine, pyridine and quinoline additions to films, respectively. This result demonstrates a simultaneous increase of both  $V_{oc}$  and  $J_{sc}$  after addition of a more basic and  $\pi$  electron rich amine to a DSSC. As a result, the overall DSSC performance increased from 2.62% for piperidine to 4.25% for pyridine and 4.63% for quinoline as-prepared films.

Conventional thermal treatment at 150 °C for 15 minutes particularly affects the performance characteristics of TiO<sub>2</sub> electrodes with heterocyclic additives (Table 2). The  $V_{oc}$  decreased following elimination of the corresponding base

Table 1 Summary of nitrogen sorption analysis for TiO<sub>2</sub> films

Films	Heat treatment	Surface area (m <sup>2</sup> g <sup>-1</sup> )	V pores <sup>a</sup> (cm <sup>3</sup> g <sup>-1</sup> )	D pores <sup>b</sup> (nm)	Porosity <sup>c</sup> (%)
Piperidine	15 minutes at 150 °C	85.3	0.253	11.9	49.6
Pyridine		87.5	0.252	11.5	49.5
Quinoline		80.4	0.254	12.6	49.7
Piperidine	30 minutes at 450 °C	79.7	0.245	12.3	48.8
Pyridine		77.6	0.246	12.7	48.9
Quinoline		75.8	0.237	12.5	48.0

<sup>a</sup> Single-point total pore volume of pores at  $P/P_0 > 0.99$ . <sup>b</sup> Average pore diameter ( $4V_A^{-1}$  by BET). <sup>c</sup>  $P = V/(\rho^{-1} + V)$ ,  $\rho$  – density of anatase ( $\rho^{-1} = 0.257$  cm<sup>3</sup> g<sup>-1</sup>).

which shifts the TiO<sub>2</sub> conduction band, resulting in a drop of 1.32, 0.66 and 1.55% for piperidine, pyridine and quinoline respectively. However, under this thermal regime TiO<sub>2</sub> particle interconnectivity occurs through dehydration of surface hydroxyls to form Ti–O–Ti bridges.<sup>22,24</sup> The formation of these bridges results in a significant rise in  $J_{sc}$  in all electrodes by 64, 15 and 16% for piperidine, pyridine and quinoline, respectively. Consequently an increase in energy conversion efficiencies of 4.21, 4.76 and 5.35% were recorded for devices with additives piperidine, pyridine and quinoline, respectively. In an attempt to improve energy conversion efficiency, the amount of quinoline additive was altered as a function of TiO<sub>2</sub> however performance remained equivalent after doubling the quantity within the paste.

On heat treatment to 450 °C, the TiO<sub>2</sub> particles undergo sintering to form robust electrodes. Both the  $J_{sc}$  and energy conversion efficiencies of all cells from the additives studied converged to  $12.3 \pm 0.2$  mA cm<sup>-2</sup> and  $6.3 \pm 0.1\%$ , respectively (Table 2). This result is attributed to necking of the TiO<sub>2</sub> nanoparticles, a reduction of defects in the semiconductor bulk, and the removal of organics at higher temperatures.

Table 2 shows a simultaneous increase of both  $V_{oc}$  and  $J_{sc}$  with more basic or richer  $\pi$ -conjugated electron heterocyclic

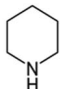
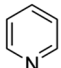
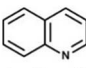
amine after no treatment and 15 minutes at 150 °C, suggesting that different surface interactions occur between the base and semiconductor and that electron transfer kinetics between the various DSSC components (TiO<sub>2</sub>, dye, electrolyte) occur when base is added during paste formulation in comparison to additions in the electrolyte.

Furthermore, dye surface concentrations were computed as  $\Gamma = A/0.001\epsilon$  from the absorbance data and scaled for the film thickness.<sup>48</sup> Minimal variation in surface coverages was observed between the three different pastes (Table 2), consistent with their similar surface areas as determined by BET measurements (Table 1). The dye forms layers with 75–95% of full monolayer coverage based on a value of  $2 \times 10^{-8}$  mol cm<sup>-2</sup>  $\mu\text{m}^{-1}$  for full coverage.<sup>49</sup>

The efficiency of four cells prepared using the quinoline based paste were tested at intervals over a 25 day period and the averaged results are shown in Fig. 6. An average decrease in efficiency of ~17% has occurred during the test period. Similar changes were recorded for cells produced from pastes prepared with pyridine and piperidine. This temporal decline in cell performance will be examined in more detail in future work.

The device  $J_{sc}$  is determined from a combination of the efficiencies for light harvesting, electron injection and electron

Table 2 Influence of heat treatment on DSSC performance for 5  $\mu\text{m}$  TiO<sub>2</sub> electrodes prepared with piperidine, pyridine and quinoline.  $\Gamma$  – dye surface concentration, [mol cm<sup>-2</sup>  $\mu\text{m}^{-1}$ ]. Average data for 4 devices

Set	Heat treatment	$V_{oc}$ [mV]	$J_{sc}$ [mA cm <sup>-2</sup> ]	FF	$\eta$ [%]	$\Gamma$
 Piperidine films	No heat treatment	753	4.84	0.72	2.62	
	15 minutes at 150 °C	743	7.95	0.72	4.21	$1.8 \times 10^{-8}$
	30 minutes at 450 °C	745	12.3	0.69	6.37	$1.6 \times 10^{-8}$
 Pyridine films	No heat treatment	760	7.51	0.75	4.25	
	15 minutes at 150 °C	755	8.63	0.73	4.76	$1.9 \times 10^{-8}$
	30 minutes at 450 °C	745	12.1	0.70	6.30	$1.6 \times 10^{-8}$
 Quinoline film	No heat treatment	772	8.12	0.74	4.63	
	15 minutes at 150 °C	760	9.39	0.75	5.35	$1.6 \times 10^{-8}$
	30 minutes at 450 °C	750	12.5	0.68	6.38	$1.5 \times 10^{-8}$
Solaronix reference	30 minutes at 450 °C	736	11.9	0.65	5.76	



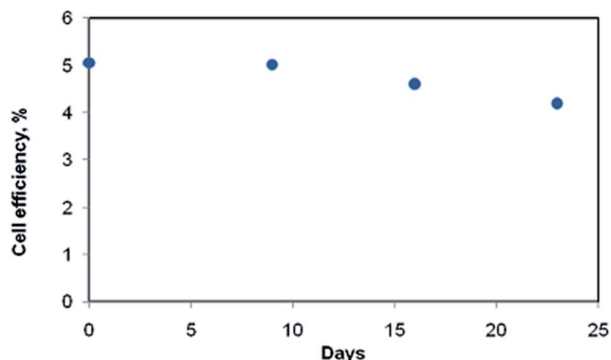


Fig. 6 Cell efficiency averaged over 4 cells produced from the quinoline based paste monitored over 25 days.

collection at the anode. In order to determine if the base in the film can improve light harvesting and potentially transfer its energy to  $\text{TiO}_2$  electrodes *via* direct charge transfer (DCT), film transmittance and the absorption spectra of the bases in solution were measured and correlated with the device incident photon-to-current conversion efficiency (IPCE) spectra. Although the  $\pi$ -aromatic bases do absorb light within the range 280–350 nm, UV-Vis spectra recorded from the different  $\text{TiO}_2$  films, at equivalent thickness, show different transmittance intensities; however there were no new absorption bands. Moreover, IPCE spectra, exhibited in Fig. 7, obtained with  $\text{TiO}_2$  electrodes sensitized with N719 show identical spectral shapes with no new bands characteristic samples preparation. We note that these IPCE spectra were measured on devices made with thin (2  $\mu\text{m}$ )  $\text{TiO}_2$  films prepared for further spectroscopic studies (*vide infra*), and thus do not match the  $J_{\text{sc}}$  data presented in Table 2. Integration of the overlap between the area under the IPCE spectra in Fig. 7 and the AM 1.5G solar spectrum does however exhibit good agreement with the  $J_{\text{sc}}$  values measured for these thin film devices (Fig. 8b). Furthermore, the ratio of  $J_{\text{sc}}$  values between the three  $\text{TiO}_2$  pastes in the thin film devices show excellent correlation with the ratio of  $J_{\text{sc}}$  values observed for the three  $\text{TiO}_2$  pastes in the devices with thicker 5  $\mu\text{m}$  films

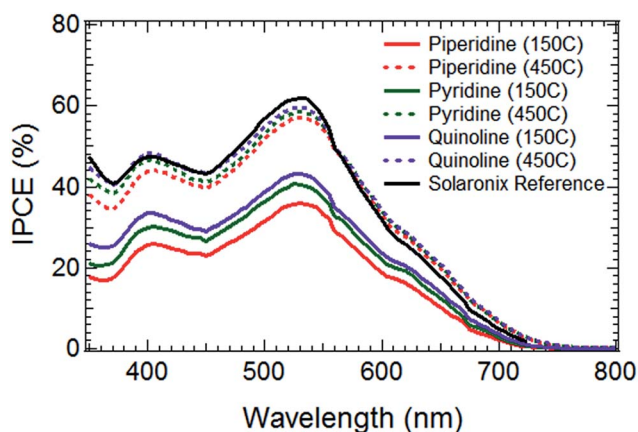


Fig. 7 IPCE of different  $\text{TiO}_2$  electrodes heat treated at 150  $^{\circ}\text{C}$  and 450  $^{\circ}\text{C}$ .

(Table 2), which indicates the device performance trends for the thin film devices are representative of the trends in the 5  $\mu\text{m}$  film devices discussed earlier. This result suggests that direct charge transfer from base additive is not apparent or at most, is not significant; therefore this observed phenomenon cannot alone explain the increases in  $J_{\text{sc}}$ .

To further investigate the  $J_{\text{sc}}$  changes in each electrode, the efficiency of charge injection from photo excited dyes into the  $\text{TiO}_2$  electrode ( $\phi_{\text{inj}}$ ) was determined by a measuring the absorbed photon to current conversion efficiency (APCE) of thin  $\text{TiO}_2$  electrodes (up to 2  $\mu\text{m}$ ). At this thickness, electron collection efficiency ( $\phi_{\text{cc}}$ ) is considered to be quantitative, and thus the APCE is indicative of the injection efficiency as described in the equations below:

$$\text{IPCE} = \text{LHE} \phi_{\text{inj}} \phi_{\text{cc}}$$

where LHE is the efficiency of light absorption by the dye.

Thus:

$$\text{APCE} = \text{IPCE}/\text{LHE} = \phi_{\text{inj}} \phi_{\text{cc}}$$

The APCE in the wavelength range of 380–620 nm, characteristic of the N719 dye absorption, of thin  $\text{TiO}_2$  electrodes are shown in Fig. 8a.

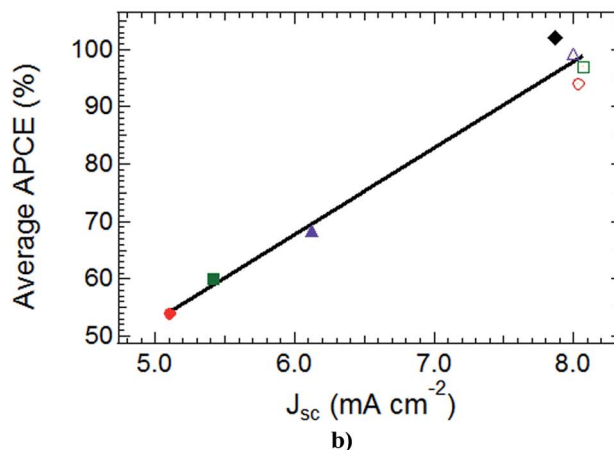
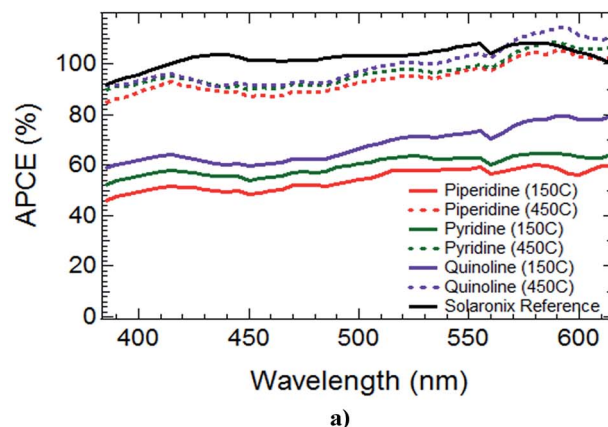


Fig. 8 (a) APCE of different  $\text{TiO}_2$  electrodes heat treated at 150  $^{\circ}\text{C}$  and 450  $^{\circ}\text{C}$ ; (b) plot of average APCE vs.  $J_{\text{sc}}$  of  $\text{TiO}_2$  electrode.

Throughout this range, at low temperature, the APCE of samples prepared using quinoline was higher than pyridine, both of which exhibit higher values than piperidine TiO<sub>2</sub> films. After sintering electrodes at 450 °C, where no organics remain within the films, the APCE of the different electrodes increased and exhibit identical values close to 100%. The APCE of these electrodes was also comparable to the one prepared from a reference device made from Solaronix paste and sintered at 450 °C. This is in agreement with previous measurements which suggest that the electron injection efficiency of N719 dye on this TiO<sub>2</sub> is close to unity.<sup>50,51</sup> This result suggests that the APCE technique employed here is an accurate way to probe the injection yield of devices. A linear relationship was found between the APCE (averaged across the spectral range) and the device  $J_{sc}$ , as shown in Fig. 8b. This provides further support to the assertion that the increased  $J_{sc}$  with the  $\pi$ -electron rich bases is likely due to the increase of APCE, and consequently electron injection.

The most commonly observed cause of changes in the injection efficiency of DSSCs is a shift in the relative driving force between the dye LUMO and the TiO<sub>2</sub> conduction band which influences the electronic overlap between the semiconductor acceptor states and the dye LUMO. To analyse whether this driving force changes with different organic bases, we first measured the dye LUMO level on TiO<sub>2</sub> films prepared with each base using cyclic voltammetry to estimate the dye HOMO and the absorbance onset of N719 to determine the HOMO–LUMO gap. The bases in the TiO<sub>2</sub> electrode were observed to have little influence on the HOMO and LUMO energies of the dye. Thus the driving force for injection is not affected by changes in the dye LUMO. To determine whether the TiO<sub>2</sub> conduction band is shifted in the presence of different bases, the relative conduction band edges were determined from transient photovoltage and charge extraction measurements (Fig. 9).

The open circuit voltage ( $V_{oc}$ ) of DSSCs was determined by the difference between the quasi-Fermi level of electrons in the nanocrystalline TiO<sub>2</sub> in the dark and under illumination. Given the high density of states in the redox mediator, its potential shifts by only  $\sim 1$  mV under illumination, thus the  $V_{oc}$  can be practically defined as the difference between the TiO<sub>2</sub> Fermi level and the Nernst potential of the redox electrolyte under illumination. Since the redox mediator is constant in all samples, the  $V_{oc}$  versus electron density plots in Fig. 9 are indicative of the relative conduction band edge potentials in each device if the energy difference between the Fermi level and conduction band edge remains constant. At 150 °C, the TiO<sub>2</sub> conduction band therefore shifts positively (with respect to an NHE reference potential) in the order piperidine < pyridine < quinoline (most positive). This positive shift corresponds to the trend in basicity of the heterocyclic amines used. This shift would cause an increase in the driving force between dye LUMO and TiO<sub>2</sub> conduction band for the more  $\pi$ -electron rich bases, and can therefore help explain the improvement in device  $J_{sc}$  observed for samples prepared from the more  $\pi$ -electron rich bases. Furthermore, the  $V_{oc}$  vs. electron density plots are coincident at 450 °C once the base is removed, supporting the

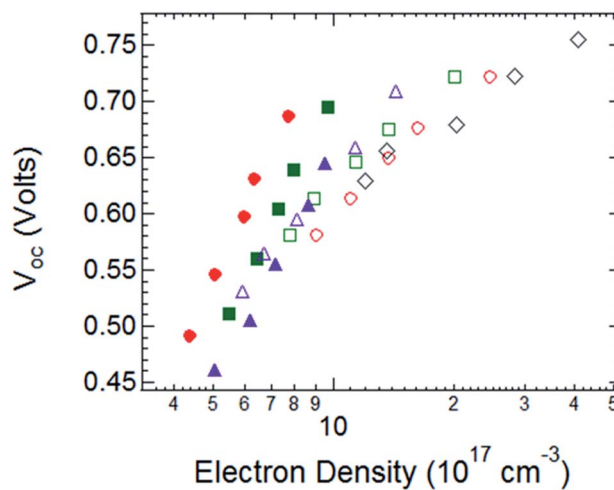


Fig. 9 Open-circuit voltage as a function of electron density in the TiO<sub>2</sub> film. Piperidine: ● – 150 °C, □ – 450 °C; pyridine: ■ – 150 °C, △ – 450 °C; quinoline: ▲ – 150 °C, ○ – 450 °C; and ◇ – Solaronix reference.

identical  $J_{sc}$  observed in these samples. We note that the slope of the plots in Fig. 9 appears to change when comparing the samples heated to 150 °C and heated to 450 °C. Since this slope is indicative of the density of trap states in the TiO<sub>2</sub>, this result suggests that the density of trap states changes after removal of the bases from the TiO<sub>2</sub>. It is therefore likely that bases contribute to trap states in the TiO<sub>2</sub>. Consequently, whilst the  $J_{sc}$  is improved by a conduction band shift increasing the driving force for charge injection, it could also be influenced by these traps in the TiO<sub>2</sub>.

The absorbance and emission measurements of Al<sub>2</sub>O<sub>3</sub> films prepared with the various heterocyclic bases and sensitized with N719 were measured (Fig. 10) in order to investigate whether the traps caused by these bases also influence the device performance. The Al<sub>2</sub>O<sub>3</sub> films were prepared using identical procedures to those for the TiO<sub>2</sub> films; however, the conduction band of Al<sub>2</sub>O<sub>3</sub> is known to be too negative to allow electron injection from N719.<sup>52</sup> Since electron injection cannot occur in these samples, they allow the dye excitation and relaxation process to be monitored directly.

Emission spectra from the films were obtained after excitation at 520 nm, with the absorbance spectra indicating identical absorption values at this wavelength. Since the number of absorbed photons is very similar and the dye is identical for all samples, the number of emitted photons would be expected to be similar. However, the emission spectra indicate that luminescence from the films with bases were quenched compared to that without any nitrogen base. Further, the films prepared with pyridine and piperidine show a greater degree of quenching compared to those prepared with quinoline. This suggests that the excited state of the dye is deactivated in the presence of the bases, an effect which is more prominent for piperidine and pyridine than for quinoline. This trend is in agreement with the previous trends observed for the injection efficiency of devices, suggesting that in addition to conduction band shifts, the  $J_{sc}$  is influenced by deactivation of the dye excited state through interaction with the organic bases.

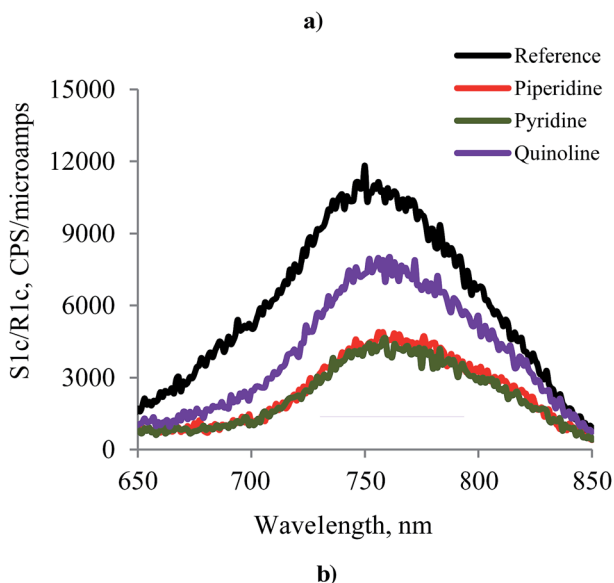
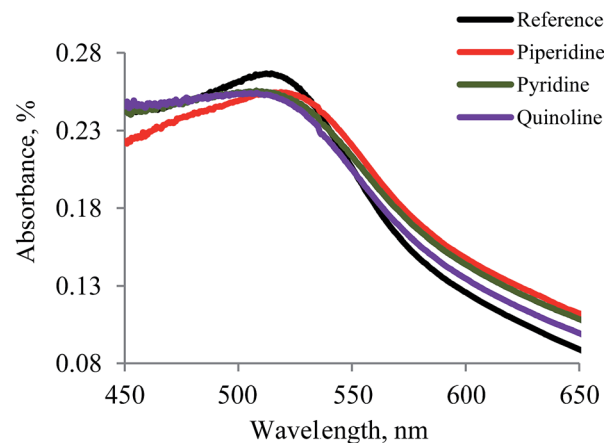


Fig. 10 (a) Absorption of N719 and (b) emission spectra of N719 excited at 520 nm for  $\text{Al}_2\text{O}_3$  films prepared with different binders.

The changes in the  $V_{oc}$  of the devices with various bases cannot be explained from the conduction band shifts observed in Fig. 9, since these show the opposite trend to that expected. However, in addition to changes in the conduction band potential, the  $V_{oc}$  can also be influenced by changes in the electron density in the film due to injection or recombination.

To investigate the transport and recombination kinetics, the electron diffusion coefficient and lifetime were determined from photocurrent and photovoltage measurements, respectively (Fig. 11). Little difference was observed in the diffusion coefficients as a function of  $J_{sc}$  between samples prepared with different bases, and the sintering temperature also did not show a large impact on the diffusion coefficients.

This indicates that the nature of the base within the electrode does not influence electron transport. However, electron lifetimes were observed to be different within the various electrodes. At low temperature, the electron lifetimes increase in the order piperidine < pyridine < quinoline when compared at the same electron density value. Since the density of traps is

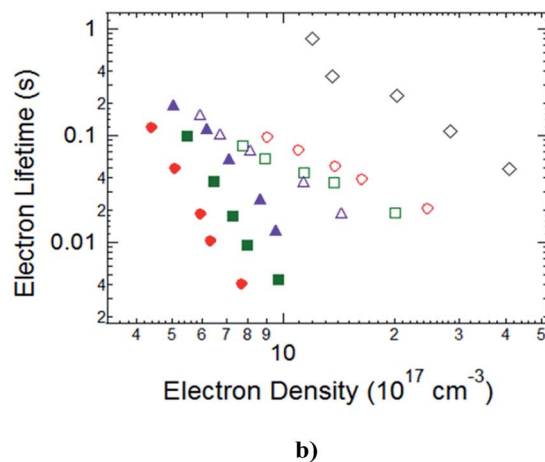
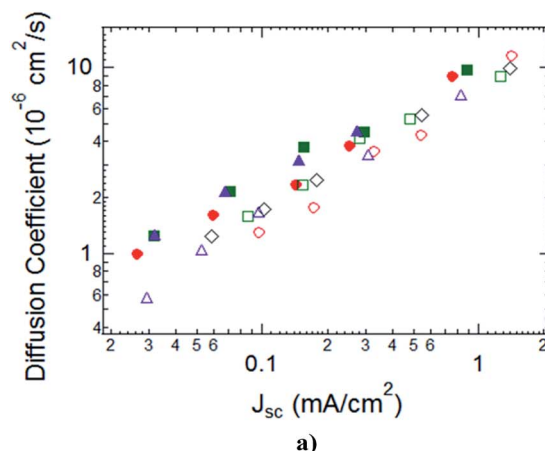


Fig. 11 (a) Electron diffusion coefficient and (b) electron lifetime of  $\text{TiO}_2$  electrodes. Piperidine: ● – 150 °C, ○ – 450 °C; pyridine: ■ – 150 °C, □ – 450 °C; quinoline: ▲ – 150 °C, △ – 450 °C; and ◇ – Solaronix reference.

comparable between the various  $\text{TiO}_2$  electrodes at 150 °C (the slopes of the  $V_{oc}$  vs. ED plots are the same in Fig. 9), these differences indicate less back electron transfer from  $\text{TiO}_2$  to the electrolyte. The origin of this effect remains ambiguous, but could be caused either by steric hindrance of the surface with bulkier bases adsorbed or by a difference in the driving force for recombination (difference between  $\text{TiO}_2$  conduction band and redox Fermi level) as the conduction band shifts between the bases. As a result of improved electron lifetime at low temperature, the device  $V_{oc}$  increases in the order quinoline > pyridine > piperidine. When the  $\text{TiO}_2$  electrodes were sintered to 450 °C, electron lifetime increases due to the reduction of  $\text{TiO}_2$  bulk defects or the removal of organics which act as traps.

Finally, a comparison of the quantity effect of quinoline added either during the paste formulation or as a component in the electrolyte is under investigation.

## Conclusions

In this study, we have demonstrated that low temperature  $\text{TiO}_2$  colloidal pastes can be prepared with heterocyclic amines to

produce robust 5 micron thick electrodes. Following a short thermal treatment of 15 minutes at 150 °C, these single cast electrodes appear to have reasonable device efficiencies even though the elimination of organic species within TiO<sub>2</sub> electrodes is not complete. A simultaneous enhancement of  $J_{sc}$  and  $V_{oc}$  has been obtained by adding a more  $\pi$ -electron rich and bulkier heterocyclic base during paste formulation instead of introduction within electrolyte. The shift of the TiO<sub>2</sub> conduction band caused by varying basicity increased the electron injection efficiency and was predominantly responsible for the  $J_{sc}$  increase. However, the bases also deactivated the dye excited state, leading to small variations in the injection yield, and a significantly lower current than when the devices were heated to 450 °C to remove the bases. The more  $\pi$ -electron rich and bulkier heterocyclic bases also resulted in higher electron lifetimes induced by less electron recombination at the interface between TiO<sub>2</sub>/dye/electrolyte, resulting in small  $V_{oc}$  enhancements.

This methodology offers significant advantages in reducing costs by allowing TiO<sub>2</sub> colloidal pastes to become the material of choice when moving to roll-to-roll printing. Furthermore, since the pastes also show efficiencies over 6% after sintering at high temperatures, they offer a high degree of versatility and could be employed on either polymer, glass or metal foil substrates in DSSCs.

## Acknowledgements

This research was carried out under funding provided by the Cooperative Research Centre for Polymers III. The authors wish to thank Dr Ian Dagley (CEO), and the participants of Project 3.1 and also acknowledge use of the facilities of Australian National Fabrication Facility (ANFF).

## Notes and references

- 1 P. B. Weisz, *Phys. Today*, 2004, **57**, 47.
- 2 S. Chu and A. Majumdar, *Nature*, 2012, **488**, 294.
- 3 T. M. Razykov, C. S. Ferekides, D. Morel, E. Stefanakos, H. S. Ullal and H. M. Upadhyaya, *Sol. Energy*, 2011, **85**, 1580.
- 4 J. Kalowekamo and E. Baker, *Sol. Energy*, 2009, **83**, 1224.
- 5 J. B. Baxter, *J. Vac. Sci. Technol., A*, 2012, **30**, 020801.
- 6 S. Ito, T. N. Murakami, P. Comte, P. Liska, C. Gratzel, M. K. Nazeeruddin and M. Gratzel, *Thin Solid Films*, 2008, **516**, 4613.
- 7 R. Harikisun and H. Desilvestro, *Sol. Energy*, 2011, **85**, 1179.
- 8 G. E. Tulloch, *J. Photochem. Photobiol., A*, 2004, **164**, 209.
- 9 B. O'Regan and M. Gratzel, *Nature*, 1991, **353**, 737.
- 10 L. M. Peter, *J. Phys. Chem. Lett.*, 2011, **2**, 1861.
- 11 J. Burschka, N. Pellet, S.-J. Moon, R. Humphry-Baker, P. Gao, M. K. Nazeeruddin and M. Gratzel, *Nature*, 2013, **499**, 316.
- 12 G. Hashmi, K. Miettunen, T. Peltola, J. Halme, I. Ashgar, K. Aitola, M. Toivola and P. Lund, *Renewable Sustainable Energy Rev.*, 2011, **15**, 3717.
- 13 T. Miyasaka, *J. Phys. Chem. Lett.*, 2011, **2**, 262.
- 14 S. Ito, P. Liska, P. Comte, R. Charvet, P. Pechy, U. Bach, L. Schmidt-Mende, S. M. Zakeeruddin, A. Kay, M. K. Nazeeruddin and M. Gratzel, *Chem. Commun.*, 2005, **34**, 4351.
- 15 T. N. Murakami, Y. Kijitori, N. Kawashima and T. Miyasaka, *J. Photochem. Photobiol., A*, 2004, **164**, 187.
- 16 D. Zhang, T. Yoshida, T. Oekermann, K. Furuta and H. Minoura, *Adv. Funct. Mater.*, 2006, **16**, 1228.
- 17 L. N. Lewis, J. L. Spivack, S. Gasaway, E. D. Williams, J. Y. Gui, V. Manivannan and O. P. Siclovan, *Sol. Energy Mater. Sol. Cells*, 2006, **90**, 1041.
- 18 J. A. Campbell, M. deBorriol, A. J. Mozer, P. J. Evans, R. P. Burford and G. Triani, *J. Vac. Sci. Technol., A*, 2012, **30**, 01A157.
- 19 H. C. Weerasinghe, P. M. Sirimanne, G. P. Simon and Y. B. Cheng, *Prog. Photovoltaics Res. Appl.*, 2012, **20**, 321.
- 20 T. Yamaguchi, N. Tobe, D. Matsumoto, T. Nagai and H. Arakawa, *Sol. Energy Mater. Sol. Cells*, 2010, **94**, 812.
- 21 M. Graetzel, R. A. J. Janssen, D. B. Mitzi and E. H. Sargent, *Nature*, 2012, **488**, 304.
- 22 N. G. Park, K. M. Kim, M. G. Kang, K. S. Ryu, S. H. Chang and Y. J. Shin, *Adv. Mater.*, 2005, **17**, 2349.
- 23 K. Kim, G. W. Lee, K. Yoo, D. Y. Kim, J. K. Kim and N. G. Park, *J. Photochem. Photobiol., A*, 2009, **204**, 144.
- 24 J. H. Yune, I. Karatchevtseva, K. Wagner, D. Officer and G. Triani, *J. Mater. Res.*, 2013, **28**, 488.
- 25 S. Y. Huang, G. Schlichthorl, A. J. Nozik, M. Gratzel and A. J. Franck, *J. Phys. Chem. B*, 1997, **101**, 2576.
- 26 G. Boschloo, L. Häggman and A. Hagfeldt, *J. Phys. Chem. B*, 2006, **110**, 13144.
- 27 H. Kusama, M. Kurashige and H. Arakawa, *J. Photochem. Photobiol., A*, 2005, **169**, 169.
- 28 H. Kusama, Y. Konishi, H. Sugihara and H. Arakawa, *Sol. Energy Mater. Sol. Cells*, 2003, **80**, 167.
- 29 H. Kusama and H. Arakawa, *J. Photochem. Photobiol., A*, 2004, **165**, 15.
- 30 H. Kusama, H. Orita and H. Sugihara, *Sol. Energy Mater. Sol. Cells*, 2008, **92**, 84.
- 31 A. M. Asaduzzaman and G. Schreckenbach, *Phys. Chem. Chem. Phys.*, 2010, **12**, 14609.
- 32 I. Karatchevtseva, D. J. Cassidy, Z. M. Zhang, G. Triani, K. S. Finnie, S. L. Cram and C. J. Barbe, *J. Am. Ceram. Soc.*, 2008, **91**, 2015.
- 33 T. X. Liu, F. B. Li and X. Z. Li, *J. Hazard. Mater.*, 2008, **155**, 90.
- 34 S. Winardi, R. R. Mukti, K. N. P. Kumar, J. Z. Wang, W. Wunderlich and T. Okubo, *Langmuir*, 2010, **26**, 4567.
- 35 N. W. Duffy, L. M. Peter, R. M. G. Rajapakse and K. G. U. Wijayantha, *Electrochem. Commun.*, 2000, **2**, 658.
- 36 S. Nakade, T. Kanzaki, Y. Wada and S. Yanagida, *Langmuir*, 2005, **21**, 10803.
- 37 H. Miyata, Y. Nakagawa, T. Ono and Y. Kubokawa, *J. Chem. Soc., Faraday Trans.*, 1983, **79**, 2343.
- 38 T. J. Dines, L. D. MacGregor and C. H. Rochester, *Langmuir*, 2002, **18**, 2300.
- 39 G. Socrates, *Infrared and Raman Characteristic Group Frequencies: Tables and Charts*, John Wiley & Sons Hoboken, NY, 3rd edn, 2004.
- 40 M. Ni, M. K. H. Leung, D. Y. C. Leung and K. Sumathy, *Sol. Energy Mater. Sol. Cells*, 2006, **90**, 1331.



- 41 K. D. Benkstein, N. Kopidakis, J. van de Lagemaat and A. J. Frank, *J. Phys. Chem. B*, 2003, **107**, 7759.
- 42 A. B. F. Martinson, T. W. Hamann, M. J. Pellin and J. T. Hupp, *Chem.–Eur. J.*, 2008, **14**, 4458.
- 43 S. K. Dhungel and J. G. Park, *Renewable Energy*, 2010, **35**, 2776.
- 44 S. Ahmed, A. Du Pasquier, T. Asefa and D. P. Birnie, *Adv. Energy Mater.*, 2011, **1**, 879.
- 45 K. S. W. Sing, D. H. Everett, R. A. W. Haul, L. Moscou, R. A. Pierotti, J. Rouquerol and T. Siemieniwska, *Pure Appl. Chem.*, 1985, **57**, 603.
- 46 T. Miyasaka and Y. Kijitori, *J. Electrochem. Soc.*, 2004, **151**, A1767.
- 47 *CRC Handbook of Chemistry and Physics, Internet Version 2005*, <http://www.hbcpnetbase.com>, ed. D. R. Lide, CRC Press, Boca Raton, FL, 2005.
- 48 M. K. Brennaman, A. O. T. Patrocinio, W. Song, J. W. Jurss, J. J. Concepcion, P. G. Hoertz, M. C. Traub, N. Y. Murakami Iha and T. J. Meyer, *ChemSusChem*, 2011, **4**, 216.
- 49 M. Grätzel, *Inorg. Chem.*, 2005, **44**, 6841.
- 50 R. Katoh, A. Huijser, K. Hara, T. J. Savenije and L. D. A. Siebbeles, *J. Phys. Chem. C*, 2007, **111**, 10741.
- 51 M. J. Griffith, A. J. Mozer, G. Tsekouras, Y. Dong, P. Wagner, K. Wagner, G. G. Wallace, S. Mori and D. L. Officer, *Appl. Phys. Lett.*, 2011, **98**, 163502.
- 52 S. E. Koops and J. R. Durrant, *Inorg. Chim. Acta*, 2008, **361**, 663.